

# Artificial Intelligence-Assisted Loop Mediated Isothermal Amplification (ai-LAMP) for Rapid and Reliable Detection of SARS-CoV-2

Mohammed A Rohaim<sup>a</sup>, Emily Clayton<sup>a</sup>, Irem Sahin<sup>a</sup>, Julianne Vilela<sup>a</sup>, Manar Khalifa<sup>a</sup>, Mohammad Al-Natour<sup>a</sup>, Mahmoud Bayoumi<sup>a</sup>, Aurore Poirier<sup>b</sup>, Manoharanehru Branavan<sup>c</sup>, Mukunthan Tharmakulasingam<sup>f</sup>, Nouman S Chaudhry<sup>f</sup>, Ravinder Sodi<sup>d</sup>, Amy Brown<sup>e</sup>, Peter Burkhardt<sup>e</sup>, Wendy Hacking<sup>e</sup>, Judy Botham<sup>e</sup>, Joe Boyce<sup>e</sup>, Hayley Wilkinson<sup>e</sup>, Craig Williams<sup>e</sup>, Michelle Bates<sup>a</sup>, Roberto La Ragione<sup>b</sup>, Wamadeva Balachandran<sup>c</sup>, Anil Fernando<sup>f</sup>, Muhammad Munir<sup>a\*</sup>

<sup>a</sup>Division of Biomedical and Life Sciences, The Lancaster University, UK; <sup>b</sup>Department of Pathology and Infectious Diseases, School of Veterinary Medicine, University of Surrey, Guildford, UK; <sup>c</sup>College of Engineering, Design and Physical Sciences, Brunel University London, Kingston Lane, Uxbridge, UK; <sup>d</sup>Department of Biochemistry, Poole & Bournemouth Hospitals NHS Trust, Longfleet Road, Poole, UK BH15 2JB; <sup>e</sup>The Royal Lancaster Infirmary, University Hospitals of Morecambe Bay NHS, Foundation Trust, UK; <sup>f</sup>Centre for Vision, Speech and Signal Processing, University of Surrey, UK.

\*Correspondence: [muhammad.munir@lancaster.ac.uk](mailto:muhammad.munir@lancaster.ac.uk)

## Abstract

Until vaccines and effective therapeutics become available, the practical way to transit safely out of the current lockdown may include the implementation of an effective testing, tracing and tracking system. However, this requires a reliable and clinically validated diagnostic platform for the sensitive and specific identification of SARS-CoV-2. Here, we report on the development of a *de novo*, high-resolution and comparative genomics guided reverse-transcribed loop-mediated isothermal amplification (LAMP) assay. To further enhance the assay performance and to remove any subjectivity associated with operator interpretation of result, we engineered a novel hand-held smart diagnostic device. The robust diagnostic device was further furnished with automated image acquisition and processing algorithms, and the collated data was processed through artificial intelligence (AI) pipelines to further reduce the assay run time and the subjectivity of the colorimetric LAMP detection. This advanced AI algorithm-implemented LAMP (ai-LAMP) assay, targeting the RNA-dependent RNA polymerase gene, showed high analytical sensitivity and specificity for SARS-CoV-2. A total of ~200 coronavirus disease (CoVID-19)-suspected patient samples were tested using the platform and it was shown to be reliable, highly specific and significantly more sensitive than the current gold standard qRT-PCR. The system could provide an efficient and cost-effective platform to detect SARS-CoV-2 in resource-limited laboratories.

**Key words:** SARS-CoV-2, diagnosis, LAMP, point of care, artificial intelligence

NOTE: This preprint reports new research that has not been certified by peer review and should not be used to guide clinical practice.

## 49 Introduction

50

51 A cluster of new pneumonia cases was reported to the World Health Organization  
52 (WHO) in late 2019 from Wuhan, Hubei Province of China. The causative agent was  
53 named as severe acute respiratory syndrome coronavirus 2 (SARS-CoV-2) and led to  
54 a global pandemic [1–3]. While the major impact of SARS-CoV-2 was attributed to frail  
55 and elderly people with co-morbidities, coronavirus disease 2019 (CoVID-19) was  
56 mainly spread by asymptomatic or mildly symptomatic patients [2]. Due to their high  
57 mutation rates and recombination events, coronaviruses can infect a range of animal  
58 species including humans, avian, rodents, carnivores, chiropters and other mammals  
59 [4]. Before the emergence of SARS-CoV-2, a total of six different coronaviruses were  
60 reported to infect humans, including HCoV-229E, HCoV-OC43, HCoV-NL63, HCoV-  
61 HKU1, MERS and SARS-CoV-1 (also known as classical SARS). The SARS-CoV-2  
62 belongs to the  $\beta$ -coronavirus of the group 2B within the family of *Coronaviridae* [3].

63

64 The SARS-CoV-2 shares a high level of genetic similarity (up to 96%) with  
65 coronaviruses originating from bats [3]. The genome of  $\beta$ -coronavirus encodes for the  
66 replicase complex (ORF1ab), spike (S), envelope (E), membrane (M) and  
67 nucleoprotein (N) genes in addition to the several non-structural and accessory  
68 proteins in the order from 5'-untranslated to 3'-untranslated regions [3]. Owing to the  
69 nature of viral genetics, the N gene is the most transcribed and highly conserved gene  
70 within the *Coronaviridae* family and has been a major target for both antigen and  
71 antibodies diagnostics. Across the genome, the RNA-dependent RNA polymerase  
72 (RdRP), encoded by the ORF1b gene segment, presents a high level of intra-group  
73 conservation and therefore is an ideal target for a diagnostic application [5, 6].

74

75 As evident by previous pandemics caused by coronaviruses, a highly specific,  
76 sensitive and easily deployable diagnostic is critical for the identification, tracing,  
77 rationalizing control measures and documentation of asymptomatic carriers and  
78 clinically evident patients [7- 9]. Additionally, due to the unavailability of the registered  
79 vaccines or effective therapeutics, rapid and reliable diagnostics are of paramount  
80 importance to curtail SARS-CoV-2 infection. Because of shortcomings associated with  
81 the virus isolation (time consuming and required containment) and cross-reactivities  
82 of antigen and antibodies assay, several real-time reverse transcription-polymerase  
83 chain reactions (qRT-PCR) and reverse-transcription loop mediated isothermal  
84 amplification (RT-LAMP) assays have been developed, validated and commercialized  
85 as useful laboratory diagnostics for the detection of SARS-CoV-2 [10]. However, the  
86 majority of these assays are time-consuming and require laboratory-intense  
87 instrumentation. Furthermore, they are unable to meet the current unprecedented  
88 rapid growth and demand for testing a large proportion of the population, identification  
89 of asymptomatic carriers and contact tracing.

90

91 Though qRT-PCR remains the gold standard for the diagnosis of SARS-CoV-2, RT-  
92 LAMP assays have been demonstrated to produce diagnostic results with increased  
93 sensitivity and specificity [11]. Furthermore, its ability to tolerate PCR inhibitors  
94 eliminates the need for laborious RNA extraction and purification methodologies [12,  
95 13]. Several platforms capable of performing LAMP assays in the field have previously  
96 been documented [14]. However, most platforms have employed fluorescence  
97 detection with integrated optical units or a smart phone dock to achieve detection [15,  
98 16]. Similarly, for colorimetric LAMP assays, smart phone cameras or user

99 interpretation of the colour changes were used to achieve detection [17, 18]. The fully  
100 integrated real-time fluorescence-based platforms are expensive, and the  
101 smartphone-based platforms are only designed for specific smartphone models.  
102 Therefore, to fulfil the need for a standalone colorimetric isothermal nucleic acid  
103 amplification platform [19], we have developed an ultra-low-cost molecular diagnostic  
104 device with an integrated single-board computer, imaging camera, artificial  
105 intelligence-based image processing algorithm and mobile app.

106  
107 In this study, we developed a high-resolution comparative genomics analysis-guided  
108 novel RT-LAMP assay for the specific and sensitive detection of SARS-CoV-2 in  
109 comparison to WHO recommended qRT-PCR assays. In order to provide a simple  
110 “sample-to-answer workflow”, an ultra-low-cost and user-friendly diagnostic platform  
111 was engineered and was further supplemented with a module for automated image  
112 acquisition and processing. Artificial intelligence-guided assessment of the LAMP  
113 assay provided faster detection of colour changes in the LAMP reaction to further  
114 enhance the assay performance and to reduce the human error in results  
115 interpretation. Finally, the assay was validated on clinical samples from CoVID-19  
116 suspected patients to demonstrate the real-life applicability.

## 117 118 **1. Material and Methods**

### 119 120 **1.1. Ethics statement**

121 This study was conducted in accordance with the University Human ethics guidelines  
122 and received a favourable review from the Faculty of Health and Medicine Research  
123 Ethics Committee (FHMREC) of Lancaster University - reference number  
124 FHMREC19112. The study was exempt from requiring specific patient consent, as it  
125 only involved the use of extracted RNA and existing collections of data or records that  
126 contained non-identifiable data about human patients.

### 127 128 **1.2. Cells and viruses**

129 Vero cells and MDCK cells were grown in Dulbecco’s modified Eagle’s medium  
130 (DMEM) (Gibco, Carlsbad, CA) supplemented with 10% inactivated foetal bovine  
131 serum (FBS) (Gibco), 2 mM L-glutamine (Gibco) and 100U/mL penicillin/streptomycin  
132 (Gibco) at 37°C in 5% CO<sub>2</sub>. Influenza A virus (A/chicken/Pakistan/UDL-  
133 01/2008(H9N2), Newcastle disease virus strain LaSota and Infectious bronchitis virus  
134 strain H120, Vesicular stomatitis virus (VSV) and Sendai virus (SeV) were propagated  
135 and used to determine the specificity of the LAMP. All viruses except influenza were  
136 titrated on Vero and MDCK cells, respectively by the standard plaque assay.

### 137 138 **1.3. *In silico* nucleotide sequence comparisons and primer design**

139 To design specific LAMP primer sets for the detection of SARS-CoV-2, all available  
140 complete genome sequences were downloaded from GISAID Initiative  
141 (<https://www.gisaid.org/>), aligned and the conserved part was selected and used as  
142 the template of LAMP primer design. To find out an efficient primer set, three sets of  
143 specific LAMP primers were hand-picked and validated using PrimerExplorer V5  
144 software (<http://primerexplorer.jp/elamp4.0.0/index.html>). Primers were validated  
145 using BLAST software (<http://www.ncbi.nlm.gov/BLAST>) to ensure their specificity.

### 146 147 **1.4. Cloning and *in vitro* transcription of RdRP target gene**

148 The coding sequence of SARS-CoV-2 RdRp gene was chemically synthesized and  
149 cloned into *pVAX1* plasmid (Invitrogen, Carlsbad, USA) between *KpnI* and *NotI*  
150 restriction sites. The plasmid was propagated in DH5 $\alpha$  cells and purified using  
151 MiniPrep Qiagen Kits. The linearized plasmid with pVAX1-RdRP was used for *in vitro*  
152 transcription using T7 RiboMAX™ Express Large-Scale RNA Production System  
153 (Promega, USA). The copy number of *in vitro* transcribed RNA was calculated from  
154 RNA concentration measured with NanoDrop™ 2000c Spectrophotometers (Thermo,  
155 USA) in triplicate. RNA products were then purified using the RNeasy MinElute  
156 Cleanup Kit (Qiagen, Valencia, CA, USA). A standard curve was generated using  
157 dilutions of the standard *in vitro* transcribed RNAs using *SuperScript III Platinum One-*  
158 *Step qRT-PCR Kit* as per the manufacturer's protocol (Invitrogen, Carlsbad, USA)  
159 using CFX384 Touch Real-Time PCR Detection System is (Applied Biosystems,  
160 USA).

161

### 162 **1.5. Clinical sample processing and spiking with miR-cel-miR-39-3p RNA**

163 A total of 199 nasopharyngeal swabs were individually collected from CoVID-19  
164 suspected patients, through routine NHS collection procedure. These samples were  
165 stored and transported in the virus transport media (VTM) to the diagnostic laboratory  
166 at Lancaster University, UK. All samples were individually spiked with 50 pmol/L of  
167 synthesized *Caenorhabditis elegans* miR-cel-miR-39-3p (Applied Biosystems/Ther-  
168 mo-Fisher Scientific, UK). The miR-cel-miR-39-3p RNA lacked any sequence  
169 homology to human or viral gene and thus present an ideal RNA extraction control.  
170 Total RNA including miRNAs was extracted using 140  $\mu$ L of the spiked-VTM by the  
171 commercial QIAampViral RNA Mini kit (QIAGEN, Valencia, California). The miR-cel-  
172 miR-39-3p RNA was used to serve as an internal control to monitor extraction  
173 efficiency and used for data normalisation. The final RNA yield and purity were  
174 determined by the A260/A280 ratio measured by a NanoDrop ND-1000  
175 spectrophotometer (NanoDrop Technologies/Thermo-Fisher Scientific, UK) with a  
176 ratio of 1.80 to 2.00 indicative of good RNA purity. The isolated RNA was stored at  
177  $-80^{\circ}\text{C}$  for further use.

178

### 179 **1.6. Real-time fluorescent-based quantitative PCR.**

180 Suspected samples with SARS-CoV-2 were tested for positivity by qRT-PCR. Briefly,  
181 RNA was extracted from Viral Transport Media using the QIAamp Viral RNA Mini kit  
182 (QIAGEN, Valencia, California) following the manufacturer instructions. The qRT-PCR  
183 was conducted using the *SuperScript III Platinum One-Step qRT-PCR Kit* as per the  
184 manufacturer's protocol (Invitrogen Carlsbad, USA) in the CFX384 Touch Real-Time  
185 PCR Detection System (Biorad, USA), according to the cycling protocol. The reaction  
186 was performed using the specific primer set RdRpF; RdRpR and FAM-labelled probe  
187 or NP-F; NP-R and ROX labelled probes designed to detect SARS-CoV2. The 25- $\mu$ L  
188 PCR reaction consists of 12.5  $\mu$ L 2X Reaction Mix, 0.2  $\mu$ M of each primer, and 0.1  $\mu$ M  
189 probe, 0.5  $\mu$ L of SuperScript® III RT/Platinum® Taq Mix, 5  $\mu$ L of RNA sample and  
190 nuclear free water. The cycling program was performed in the CFX384 Touch Real-  
191 Time PCR Detection System is (Applied Biosystems, USA), according to the cycling  
192 protocol. The amount of viral RNA in each sample was estimated by comparing the  
193 cycle threshold values (Ct) to the standard curve made by serial 10-fold serial dilutions  
194 of previously titrated *in vitro* transcribed RdRP gene.

195

### 196 **1.7. ai-LAMP assay performance**

197 All experiments for LAMP were run in triplicate. The LAMP reactions were performed  
198 using WarmStart™ Colorimetric LAMP 2X Master Mix (New England Biolabs). A 10X  
199 primer mix (FIP, 16 µM; BIP, 16 µM; F3, 2 µM; B3, 2 µM; LF, 4 µM; LB, 4 µM) was  
200 prepared. A 25 µl reaction mixture (12.5 µl 2X MasterMix; 2.5 µl 10X primer mix; 2.5  
201 µl RNA and 7.5 µl DNase & RNase-free molecular grade water) was mixed  
202 homogeneously and centrifuged. The LAMP was performed in a thermocycler  
203 (MJResearch) at 65°C for 30 min or in the engineered device (**Figure 4A**). Colour  
204 change was observed directly by the naked eye or through image processing, and  
205 agarose gel electrophoresis was performed to confirm the results. The completion of  
206 amplification was indicated by the colour in the tube, wherein yellow was considered  
207 positive and pink was regarded as negative. The amplicon was confirmed by 2%  
208 agarose gel electrophoresis.

209

### 210 **1.8. Artificial intelligence based test-tube colour detection**

211 A loop-mediated isothermal amplification (LAMP) assay based COVID-19 test device  
212 was proposed to obtain the COVID-19 test results in 30 minutes based on colour  
213 changes. Artificial intelligence (AI) based colour detection was proposed to identify  
214 colour changes considering different lighting issues and to reduce the test running  
215 time less than 30 minutes. Images were acquired from the COVID-19 test kit which  
216 carried 8 test-tubes including NTC (negative test control) and PTC (positive test  
217 control) for every 20 seconds during the test operation. Each image was cropped into  
218 separate tubes using template matching approach and labelled manually based on  
219 their colour.

220

### 221 **1.9. Analytical specificity and analytical sensitivity of LAMP**

222 The designed RdRp primer sets for LAMP to detect SARS-CoV-2 were validated for  
223 their specificity by testing the cross-reactivity with other viruses, including influenza A  
224 virus, Vesicular stomatitis virus (VSV), Sendai virus (SeD), infectious bronchitis virus  
225 (IBV) and Newcastle disease virus (NDV). Likewise, the developed LAMP assay was  
226 evaluated to test the primers set sensitivity in a serially diluted standard RNA template  
227 prepared by tenfold serial dilutions. The amplification patterns were observed for each  
228 dilution to determine the lowest amount of absolute RNA template required for  
229 detectable amplification. The degree of colour intensity of the amplified product as well  
230 as the observed electrophoretic pattern during gel electrophoresis was used for the  
231 analysis of LAMP amplification.

232

### 233 **1.10. Quantitative real time PCR for miR-cel-miR-39-3p RNA**

234 In order to determine the RNA extraction efficiency, the extracted RNA was reverse  
235 transcribed using a commercially available kit (Applied Biosystems/Thermo-Fisher  
236 Scientific, UK) using miR-specific stem-loop primers as per manufacturer instructions.  
237 A total of 5 µL of the sample was added to a 96-well plate together with 10 µL reaction  
238 mixture (MasterMix™) containing along with Multiscribe™ reverse transcriptase (50  
239 U/µL), and 0.19 µL RNAase inhibitor (20 U/µL). The RT reaction was performed at 16  
240 °C for 30 min, followed by 42 °C for 30 min, and 85 °C for 5 min and was finally kept  
241 at 4 °C. A NTC was considered in every individually run reaction to identify any  
242 unspecific amplification. The RT products were quantified immediately by qPCR using  
243 TaqMan™ MicroRNA assays (Applied Biosystems/Thermo-Fisher Scientific, UK) in  
244 a 96 well plate using the 7900HT Fast Real-Time PCR System (Applied Biosystems,  
245 UK) as we described before [37]. The quantification cycle (Cq) was determined with

246 instrument default threshold settings (10 SDs above the mean fluorescence of the  
247 baseline cycle).

248

### 249 **1.11. Statistical analysis**

250 GraphPad Prism Software version 6.01 for Mac (GraphPad Software, La Jolla,  
251 California, USA) was used for graphs generation. The LAMP detection sensitivity and  
252 specificity were calculated using the chi-squared test. TPR (true positive rate), TNR  
253 (true negative rate), FPR (false positive rate), FNR (false negative rate) were  
254 calculated according to the following equations:  $TPR = TP / (TP + FN)$ .  
255  $TNR = TN / (FP + TN)$ .  $FNR = FN / (TP + FN)$ .  $FPR = FP / (FP + TN)$ . TP: total number of true  
256 positives. TN: total number of true negatives. FN: total number of false negatives.  
257

258

## 259 **2. Results**

260

### 261 **2.1. High resolution conversation analysis of SARS-CoV-2 to guide promising 262 oligos design**

263 It is imperative to critically assess the evolving nature of viruses in identifying  
264 conserved gene signatures and guiding the selection of the most appropriate primers.  
265 In order to identify important genomic loci, we downloaded and aligned all the available  
266 full-length genomes with high coverage sequences ( $n=22858$ ) of SARS-CoV-2 by  
267 Multiple Alignment using Fast Fourier Transform (MAFFT) [20]. We then compiled *in*  
268 *house* R-code (available on request) to determine the single nucleotide-based genetic  
269 conservation across the length of ~30kb genome. The analysis of the aligned dataset  
270 of all genomes in the RStudio generated a total of 18GB high-resolution nucleotide-  
271 by-nucleotide score from 0.0 to 1.0 (1.0 being the highly conserved and 0.0 being the  
272 highly divergent). Plotting the assessed genetic divergence, at a cut point of 90%  
273 similarity along with the genome of the SARS-CoV-2, identified sharp divergence at  
274 multiple loci (**Figure 1A**). However, most of the genomes maintained high  
275 conservation. The divergence at the 5' and 3' ends was primarily due to length  
276 heterogeneity, which may be partly as a result of sequencing artifact or potentially  
277 coronaviruses ragged termini (**Figure 1B**). Owing to high divergence, a stretch of  
278 sequence (~400 nucleotides, numbering corresponds to the complete genome of  
279 strain SARS-CoV-2/human/USA/VA-DCLS-0285/2020 strain, GenBank Accession  
280 Number: MT558705.1) spanning the start of the ORF1b, which encode for viral RNA-  
281 dependent RNA polymerase (RdRP), was targeted to design oligos for the LAMP  
282 assay. Additionally, this specific target genomic locus was adjacent to oligos  
283 recommended by the World Health Organization (WHO) and Public Health England  
284 (PHE) for real-time RT-PCR-based routine identification of CoVID-19 patients, further  
285 allowing direct and comparable evaluation of real-time RT-PCR with *de novo*  
286 developed LAMP assay (**Figure 1C**).

287

288 The conserved region of the RdRP gene with the lowest mutation frequencies was  
289 used as a template to manually design three sets of basic LAMP primers and selected  
290 with PrimerExplorer V5 for appropriate primer lengths, loop selection and melting  
291 temperature optimization (**Figure 1C**). In order to preclude the non-specific  
292 amplification of common coronaviruses, efforts were made to design primers in the  
293 regions where there is a high level of divergence among more than 3 of the 6 total  
294 primers in a specific set. Amongst the most suitable targets, the primers with high  
295 scores were aligned with MERS-CoV, hCoV-229E, hCoV-OC43, hCoV-NL63, hCoV-

296 HKU1 and SARS-CoV-1 (**Figure 1D**). These selected primers were used for further  
297 validation and screening.

298

## 299 **2.2. Determination of limit of detection using biochemically synthesis RNA**

300 In order to assess the robustness of the primers, we used a fully identical *in vitro*  
301 transcribed target RNA unanimously spanning the length of the RdRP-gene based  
302 LAMP and qRT-PCR target regions. The pre-determined copy numbers of the  
303 biochemically synthesised RNA were 10-fold serially diluted from  $10^7$  copies to 0  
304 copies of the target gene per reaction. To determine the analytical sensitivity of the  
305 assays, we first evaluated their limits of detection (LoD) for both qRT-PCR and LAMP  
306 assays. The LoD of the qRT-PCR was 10 copies as evident from the relative  
307 fluorescence units (**Figure 2A**) and electrophoreses of the amplified products (**Figure**  
308 **2B**). The standard curve generated by the RdRP-based qRT-PCR was linear and  
309 generated a coefficient of correlation ( $R^2$ ) = 0.9481 and a slope of -2.6509 (**Figure**  
310 **2C**). Melting curve analysis revealed the specificity of primers for the target gene  
311 sequence, as all the amplified products showed a uniform melting temperature ( $T_m$ )  
312 of  $\sim 75.10^\circ\text{C}$  and specific amplification patterns (**Figure 2B** and data not shown).  
313 Compared to the qRT-PCR assay, the LoD for the LAMP which targeted the same  
314 RdRP gene was 1 log unit higher ( $10^2$  copies/reaction) (**Figure 2D**, upper panel) as  
315 assessed by visual observation of the LAMP reaction, where positive reactions turned  
316 yellow and negative reactions remained pink when observed by the naked eye. To  
317 further confirm the specific amplification of the target region, the gradient LAMP  
318 products were visualized by DNA staining and gel electrophoresis for the amplified  
319 product, further confirming the detection limit of LAMP (**Figure 2D**, lower panel).

320

## 321 **2.3. Specificity of the novel LAMP with other respiratory and medically** 322 **important viruses**

323 The SARS-CoV-2 embraces genetic and phenotypic features of several common cold  
324 coronaviruses and other viruses of the respiratory tract. Owing to high genetic  
325 similarity (up to 96% at nucleotide levels) and common respiratory specimen for  
326 clinical identification of CoVID-19 patients, we aimed to investigate any non-specific  
327 amplification in the LAMP assay. In order to demonstrate the specificity of the LAMP  
328 assay, we used pathogens belonging to 5 families of the most important medical and  
329 respiratory viruses. As shown in the **Figure 3A**, the qRT-PCR specifically detected  
330 only the SARS-CoV-2 and this specificity was noticed on Gel-red staining of amplified  
331 products (**Figure 3B**). Consistently, no cross-reactivities were noticed with the LAMP  
332 in both colorimetric detection (**Figure 3C**, upper panel) or electrophoreses (**Figure 3C**,  
333 lower panel). Collectively, a high level of specificity was observed in primers set using  
334 either of the assays.

335

## 336 **2.4. Temporal investigations of the LAMP and its impact on the limit of detection**

337 One of the major advantages of LAMP is its robustness. In order to determine the time  
338 optimal for sufficient amplification of targeted genes, *in vitro* transcribed RNA was used  
339 as a template for 30 minutes and assessed after every 5 minutes post-start of the  
340 reaction. The change in colour was monitored visually by the naked eye. As shown in  
341 Table 1, under equivalent conditions similar results were obtained from 20-30 minutes  
342 of amplification. Therefore, 30 min was selected as the optimal visual interpretation  
343 time for the results.

344

345 While the change in colour, reflective of a positive reaction, could be detected as early  
346 as 20 minutes post-start of the reaction at lower copy number, subjective variabilities  
347 may result in erroneous interpretation, especially in colorimetric based diagnostic  
348 assays. To propose an automated imaging, processing and interpretation of the LAMP  
349 based results, we developed a user-friendly device and furnished it with an artificial  
350 intelligence based automatic interpretation algorithm.

351

## 352 **2.5. Manufacture of an isothermal nucleic acid amplification device with** 353 **colorimetric detection features**

354 A device (**Figure 4A**) was built with many off-the-shelf electronic components and  
355 custom flexible resistive heating elements (5W, NEL, UK), and specially designed  
356 aluminium heating blocks. Raspberry Pi (RPI) was used to control the device. The one  
357 wire interface of the RPi was used to connect ten digital temperature sensors  
358 (DS18B20, Maxim Integrated, USA) positioned directly on the PCB boards to monitor  
359 heater block temperature changes and provide feedback control. The specially  
360 designed aluminium heater blocks to hold 200  $\mu$ l PCR tubes and the lid heater to  
361 prevent condensation were attached directly on top of the surface mount temperature  
362 sensors on the respective PCBs with a heat transferring adhesive (TermoGlue,  
363 Termopasty Grzegorz Gasowski, Poland). The flexible resistive heating elements  
364 were also attached to the heater blocks. To circumvent the need for specialised docks  
365 and eliminate user interpretation of the colorimetric results, a Raspberry Pi Camera  
366 (RPi Camera) was used. Eight LEDs (LW T733, Osram, Germany) were assembled  
367 on the top side of the lid mount PCB to shine light directly into the reaction tubes to  
368 achieve consistent lighting within the device. All the above components were  
369 assembled into a 3D printed enclosure (14.3 x 10.8 x 6 cm) specially designed with  
370 openings to access to the USB and TCP/IP ports of the RPi. A 20,000 mAh power  
371 bank (Anker Power Core, Anker, China) with two 5V, 2A output was used to power the  
372 device. A Python based control software was used to control the heating, image the  
373 progression of the LAMP assay and store the 'time-lapse' images and temperature  
374 data within a specified folder. The user can initiate a test by either connecting to a  
375 screen via the HDMI port or through simply pairing the device with the mobile app via  
376 Bluetooth and selecting the required diagnostic assay.

377

## 378 **2.6. Automated image acquisition and processing through template matching-** 379 **based algorithm**

380 The LAMP assay in 8 separate tubes was remotely started to initiate heating to 65°C.  
381 Images of those test tubes were captured using the inbuilt RPi Camera for every 20  
382 seconds and were saved in the RPi in the RGB format. Each individual image  
383 consisted of 8 frames around each tube with a black background. As the tube area  
384 exposing colour changes was fractionally small compared to its background, we first  
385 extracted each targeted tube frame from the image before applying an image  
386 processing algorithm. In order to process these extracted frames, a reference tube  
387 was selected as a template, and a template matching algorithm [21] was applied to  
388 extract all tubes from the first image. The rationale for the template matching was to  
389 search and find the location of a template image in a larger image. It simply slides the  
390 template image over the input image to perform the 2-dimensional convolution and  
391 compared values to get the maximum overlap to decide the exact similar areas.  
392 Assuming that positions of the test-tube do not change over the time of an experiment,  
393 images were cropped in an experiment to obtain the tube frames from the entire  
394 image. These crops are then saved into a 2-dimensional array for RGB colour space



395 (see equation below). Once extracted, RGB format images were converted to YUV  
396 format using the following transformation [22] to avoid diffraction and lighting  
397 variabilities in different images.

398

$$399 \quad \begin{pmatrix} Y \\ U \\ V \end{pmatrix} = \begin{pmatrix} +0.257 & +0.504 & +0.098 \\ -0.148 & -0.291 & +0.439 \\ +0.439 & -0.368 & -0.071 \end{pmatrix} \cdot \begin{pmatrix} R \\ G \\ B \end{pmatrix} + \begin{pmatrix} 16 \\ 128 \\ 128 \end{pmatrix}$$

400

401 In YUV colour space, the Y channel represented the luminance of the colour, while  
402 the U and V channels represented the chrominance (**Figure 4B**). Separating the  
403 luminance from the chrominance reduced the effect of light changing and shadow  
404 noises in each tested tube [23]. Finally, the chrominance (U, V) channels from the  
405 YUV image were considered for image processing. The chrominance (U, V) values of  
406 those extracted test tubes were compared with reference orange test tubes in positive  
407 control and reference pink image in negative control test tubes to calculate the sum of  
408 absolute difference (SAD) for each of the pixel values. After experiments with two  
409 images set and fine tuning the threshold values manually, a SAD threshold value was  
410 achieved which provides 100% accuracy in the separation of classes.

411

412 Despite the SAD based approach resulting in 100% accuracy for the images after 30  
413 minutes, this approach failed with other datasets containing bubbles and different  
414 background lights as a different threshold value was produced for each image set.  
415 Therefore, a deep learning-based approach was utilised in our experiments to  
416 generalize the classification for different background light and sound sources.

417

## 418 **2.7. Artificial intelligence-assisted rapid detection of colour changes** 419 **associated with the LAMP reaction**

420 Multiple rule-based computer vision techniques were applied to identify small changes  
421 in light intensity and to fix the position. Deep learning is a subdomain of AI which  
422 doesn't require any domain knowledge to work, however, it learns hidden patterns  
423 from examples present in the dataset. A deep learning Convolutional Neural Network  
424 (CNN) [24] architecture was proposed with the bespoke 8 layers deep mode as shown  
425 in **Figure 4C**. It consisted of four convolutional layers followed by 2 dense and an  
426 output layer. To compile the model, binary cross-entropy was used as a loss of  
427 function and used to optimize.

428

429 For the training of the network, the dataset was shuffled and then split into 9:1  
430 proportion (**Figure 4D**). 90% of the data was used to train the network and the  
431 remaining 10% was exploited to check how the network behaved on seeing a new  
432 image. Training a dataset requires loading numerous images into the memory in a  
433 single operation which is an expensive process. Therefore, a data generator was  
434 implemented that read the data in batches from the dataset directory and fed it to the  
435 model. After multiple experiments, it was observed that the network converged after 6  
436 cycles (epochs) through the dataset. Therefore, we ran an experiment for only 6  
437 epochs to decrease the probability of overfitting. In addition, an additional set of 108  
438 test-tube crops was used to validate the network. The best performing network  
439 resulted in an accuracy of 98% in classifying tubes based on their colours (images  
440 with better light).

441

442 In order to assess the temporal impact of the AI-assisted detection of colour changes  
443 (indicative of amplification), the RT-LAMP reaction was run with 3 previously  
444 confirmed positive and negative patient samples as well as positive and negative  
445 controls. Colour changes were assessed every 5 minutes until the complete stoppage  
446 of the LAMP reaction at 30 minutes. Gradual colour changes were detectable with the  
447 naked eye as early as 20 minutes post-start of the reaction (**Figure 5A**).  
448 Corresponding samples were run on the newly developed device and temporal and  
449 real-time colour changes were monitored as described earlier. Depending upon the  
450 viral load in the sample, a clear colour change was calibrated as early as 20 minutes  
451 using device operated processing of the data (**Figure 5B**). Once the positive test  
452 control is identified as positive, the test will be stopped, and results will be returned to  
453 reduce the waiting time and power consumption on heating.

454  
455 As shown in Fig 5B, template matching algorithm is applied to extract test tubes and  
456 CNN model is applied and trained. The CNN model is used as machine learning  
457 algorithm to identify colours for each image taken throughout the experiment. Images  
458 taken at time tare marked as 't' in the Fig 5B. Once positive control test and negative  
459 control test give the correct results consecutively for three times, LAMP based test will  
460 be stopped, and results will be returned. This approach will reduce the waiting time for  
461 the results and power consumption due to heating in the experiment.

## 462 **2.8. Validation of ai-LAMP and comparative performance in clinical settings**

463 In order to assess the field application of the optimized assay, we applied the ai-LAMP  
464 to purified RNA spiked with miR-cel-miR-39-3p from CoVID-19 patients. A total of 199  
465 swab samples were collected from CoVID-19 clinically suspected patients during  
466 routine screening at the Royal Lancaster Infirmary (RLI), University Hospitals of  
467 Morecambe Bay NHS Foundation Trust UK. The extracted RNA from swab samples  
468 were run in parallel for ai-LAMP and two WHO/PHE recommended qRT-PCR targeting  
469 the RdRP and N genes of the SARS-CoV-2. This parallel assessment allowed us to  
470 assess the comparative performance of the ai-LAMP.

471  
472 The RdRP gene-based qRT-PCR detected a total of 67 positives and 132 negatives  
473 in a cohort of 199 patients (**Figure 6A**). In contrast, a higher number of positive (n=88)  
474 and lower numbers of negative (n=111) were detected by the qPCR which targeted  
475 the N gene (**Figure 6B**). Interestingly, the ai-LAMP detected a total of 126 positive  
476 samples which constituted several times higher than RdRP and N gene-based qPCR,  
477 respectively. Comparative analysis of these three molecular detection assays  
478 revealed 58 total true positives (TP), 09 false negatives (FN), 64 true negatives (TN),  
479 and 68 false positives (FP) in RdRP-based qRT-PCR compared to RdRP-based  
480 LAMP (**Figure 6A**). Similarly, upon comparative analysis of the N gene-based qPCR  
481 and RdRP-based LAMP, we observed a total of 74 TP, 14 FN, 59 TN, and 52 FP  
482 (**Figure 6B**).

483  
484 In the current clinical settings, a qRT\_PCR targeting two genes (N and RdRP) was  
485 conducted to conclusively identify CoVID-19 positive cases and this assay is referred  
486 as cumulative (CUM) qRT-PCR. In this scenario, a sample would be considered as  
487 positive only if a Ct value of  $\geq 35$  was detected in both N and RdRP-gene based  
488 qRT-PCR. Using this approach, we noticed a total of a 70 positive and 129 negative  
489 samples and an improved true positive (n=61), false negatives (n=09), true negatives  
490 (n=64), and false positives (n=65) limits (**Figure 6C**). Taken together, the cumulative  
491

492 comparative picture of the qPCR and ai-LAMP has identified a superior detection of  
493 positive cases (**Figure 6D**). In order to confirm this detection performance, all ai-LAMP  
494 amplification products were visualised by electrophoresis (data not shown), further  
495 confirming the aided-detection and improved implication of ai-LAMP in the field  
496 condition.

497  
498 We next determined the detection limit of the ai-LAMP in direct correlation with the  
499 standard Ct values of the qPCRs. Plotting of ai-LAMP positive and negative data  
500 against the linearity of the Ct values revealed that ai-LAMP carried Cp (cycle number  
501 at detection threshold) of up to 37 Ct determined in the qPCR based on the RdRP  
502 gene (**Figure 6E and Supplementary Table 1**) or N gene (**Figure 6F and  
503 Supplementary Table 1**) of the SARS-CoV-2. This detection is approximately 2 Ct  
504 values higher than the detection limit of the standard qPCR. Analysis of the first 96  
505 samples, run in parallel for the ai-LAMP, (**Figure 6G and Supplementary Table 1**)  
506 showed a clear demarcation of the positive and negative samples in the RdRP-gene  
507 based ai-LAMP. In order to rule out the quantitative recovery from spiked miRNA, a  
508 qRT-PCR was run for 40 randomly selected samples [37]. Based on the Ct values, all  
509 samples showed a marked recovery except a single sample where a low detection of  
510 the miRNA was identified (**Figure 6H, Supplementary Table 1 and Supplementary  
511 Figure 1**).

512  
513 Collectively, these data highlight the improved specificity and sensitivity of the AI-  
514 assisted LAMP assay compared to the naked-eye interpretation of the LAMP-  
515 positivity, thus enhancing the timely and automated detection and interpretation of the  
516 assay results.

517

### 518 **3. Discussion**

519

520 The SARS-CoV-2 is now a global pandemic, over 216 countries are currently reporting  
521 active infections around the globe and the number of daily infections and deaths is  
522 continuing to increase, especially in the Americas and South East Asia in a series of  
523 multiphasic spread [25]. Currently, there is no licensed vaccine or registered drugs,  
524 leaving timely identification of CoVID-19 patients, contact tracing and isolation of  
525 positive contacts as the most effective means of containing the pandemic. Among  
526 different molecular diagnostic chemistries, the LAMP technology provides a promising  
527 approach for rapid and reliable detection in resource-limited settings [14]. Recently,  
528 the LAMP technology has been widely applied for the identification of West Nile virus,  
529 influenza virus, yellow fever virus, Marburg virus, Ebola virus, Zika virus, and other  
530 myriads of viruses [26- 31].

531

532 The genome of SARS-CoV-2 is approximately 30kb in size with a coding capacity of  
533 9860 amino acids. All of the  $\beta$ -coronaviruses encodes for structural (replicases, S, E,  
534 M and N) genes in the order of 5' to 3' in the positive sense genome [5, 32, 33]. A  
535 range of qRT-PCRs have been proposed and are referred by the World Health  
536 Organization [25; [https://www.who.int/emergencies/diseases/novel-coronavirus-  
537 2019/technical-guidance/laboratory-guidance](https://www.who.int/emergencies/diseases/novel-coronavirus-2019/technical-guidance/laboratory-guidance)] for diagnosis of SARS-CoV-2. While  
538 diagnostic assays can be designed on the most conserved region of the viral genome,  
539 most of the routinely applied RT-PCR and RT-LAMP have been targeting the S, N,  
540 RdRP, and ORF1a/b genes mainly due to their high level of transcription and  
541 abundance in expression compared to other genes of the SARS-CoV-2 [5, 6]. For the

542 detection of SARS-CoV-2, Chan et al., [34] have targeted and developed a standard  
543 RT-LAMP with LoD of 11.2 RNA copies/reaction using *in vitro* RNA transcripts. Yan et  
544 al., [13] have adapted the ORF1ab to developed RT-LAMP assay with a detection limit  
545 of sensitivities of  $2 \times 10^1$  copies per reaction. The majority of these diagnostic assays  
546 carry a high level of sensitivity, specificity and repeatability; however, these primarily  
547 lack the clinical validation and/or optimization on the synthetic targets.

548  
549 In this study, we have developed and evaluated a novel RT-LAMP in one of the most  
550 conserved genes (i.e. RdRP) within the SARS-CoV-2 genome. The RT-LAMP was  
551 then directly compared with the currently applied routine diagnostic assays to assess  
552 the comparative performance. The RT-LAMP assay developed in this study, could  
553 detect as low as 100 copies with an *in vitro* RNA transcript. Importantly, the RT-LAMP  
554 has detected the SARS-CoV-2 RNA in 68/199 (34%) and 52/199 (26%) additional  
555 specimens that were tested negative by the RdRP-based qRT-PCR and N-based  
556 qRT-PCR, respectively. These findings are interesting, both clinically and  
557 epidemiologically due to the high proportion of asymptomatic and mildly symptomatic  
558 cases of CoVID-19. These apparently healthy people have been suggested as major  
559 sources of virus propagation and basis of epidemics within the community [34, 35, 36].  
560 Due to the large number of cases (~5000) in the testing facility, additional positive  
561 specimens could have been detected by the RT-LAMP which might have remained  
562 undetected by the qRT-PCRs. Using of an internal standard that is not expressed in  
563 humans such as cel-miR-39-3p can alleviate the problem of an effective RNA  
564 extraction approach. In addition, we used a fixed total RNA concentration in all  
565 experiments allowing for better comparisons across groups.

566  
567 The main challenges of using the Colorimetric approach are background which  
568 changes the colour perspective, issues in identifying small changes, bubbles in the  
569 test tubes, relatively small area corresponding to colour change and pixel variation  
570 due to camera flash and background reflections. The CNN based model has used  
571 high-performance computer images to train using these issues and having learned the  
572 patterns is able to classify colour, despite the presence of noise. The trained model  
573 has successfully moved to Rpi to identify colour changes in test tubes. The study  
574 produced 98% accuracy for images taken with better light (Open) and the duration of  
575 testing could be dynamically controlled to reduce the length of operating time and  
576 heating with a resulting reduction in energy consumption by the device.

577  
578 Collectively, our data showed that the newly established ai-LAMP was highly specific  
579 for the detection of SARS-CoV-2 RNA *in vitro* and in respiratory tract clinical  
580 specimens. The usage of this novel LAMP assay might be helpful especially for  
581 detecting COVID-19 cases with low viral loads and when testing upper respiratory tract  
582 specimens from patients. Development of ai-LAMP into a multiplex assay which can  
583 simultaneously detect other human-pathogenic coronaviruses and respiratory  
584 pathogens may further increase its clinical utility in the future.

## 585 586 **Acknowledgements**

587 The authors would like to thank the Electronic Technicians William Schkzhamian,  
588 Gopalakirishnan Jeysundra and Michael Lateo of Brunel University London for their  
589 efforts to come into the University with special permission during the early lockdown  
590 period to produce eight laboratory prototypes within 5 days. We thank the Microbiology  
591 Department, University Hospitals of Morecambe Bay for access to anonymised patient

592 samples and acknowledge the support of BLS Lancaster University Technicians  
593 throughout the lockdown period. We would like to thank Dr Derek Gatherer, Lancaster  
594 University, in aligning large SARS-COV-2 genome sequences.

#### 596 **Disclosure statement**

597 No potential conflict of interest was reported by the authors.

598

#### 599 **Funding**

600 The authors wish to express our sincere appreciation to the BBSRC for allowing us to  
601 repurpose the LAMP prototypes produced in the grant BB/R012695/1 to be used for  
602 SARS-CoV-2 laboratory testing at The University of Lancaster. We would like to thank  
603 the support of BBSRC (BB/M008681/1 and BBS/E/I/00001852) and British Council  
604 (172710323 and 332228521) at Division of Biomedical and Life Sciences, Lancaster  
605 University, UK. We would also like to thank Brunel University London and the  
606 University of Surrey for providing some financial support to rapidly produce these  
607 devices.

608

#### 609 **References**

610

611 [1] Zhu N, Zhang D, Wang W, et al. A novel coronavirus from patients with pneumonia  
612 in China, 2019. *N Engl J Med*. 2020 Feb 20;382(8):727-733.

613 [2] Chan JF, Yuan S, Kok KH, et al. A familial cluster of pneumonia associated with  
614 the 2019 novel coronavirus indicating person-to-person transmission: a study of a  
615 family cluster. *Lancet*. 2020a;395:514–523.

616 [3] Zhou P, Yang XL, Wang XG, et al. A pneumonia outbreak associated with a new  
617 coronavirus of probable bat origin. *Nature*. 2020 Mar;579(7798):270-273.

618 [4] Decaro N and Lorusso A. Novel human coronavirus (SARS-CoV-2): A lesson from  
619 animal coronaviruses. *Vet Microbiol*. 2020 May;244:108693.

620 [5] Chan JF, Kok KH, Zhu Z, et al. Genomic characterization of the 2019 novel human-  
621 pathogenic coronavirus isolated from a patient with atypical pneumonia after visiting  
622 Wuhan. *Emerg Microbes Infect*. 2020; 9(1): 221–236.

623 [6] Kim D, Lee J, Yang J, et al. The Architecture of SARS-CoV-2 Transcriptome. *Cell*.  
624 2020 May 14;181(4):914-921.e10.

625 [7] Peiris JS, Lai ST, Poon LL, et al. Coronavirus as a possible cause of severe acute  
626 respiratory syndrome. *Lancet*. 2003 Apr 19;361(9366):1319-25.

627 [8] Woo PC and Yuen KY. Severe acute respiratory syndrome coronavirus as an agent  
628 of emerging and reemerging infection. *Clin Microbiol Rev*. 2007 Oct; 20(4): 660–694.

629 [9] Yuen KY. Middle East respiratory syndrome coronavirus: another zoonotic  
630 betacoronavirus causing SARS-like disease. *Clin Microbiol Rev*. 2015 Apr;28(2):465-  
631 522.

632 [10] WHO, Novel Coronavirus – China 2020a. [https://www.who.int/csr/don/12-january-  
633 2020-novel-coronavirus-china/en/](https://www.who.int/csr/don/12-january-2020-novel-coronavirus-china/en/)

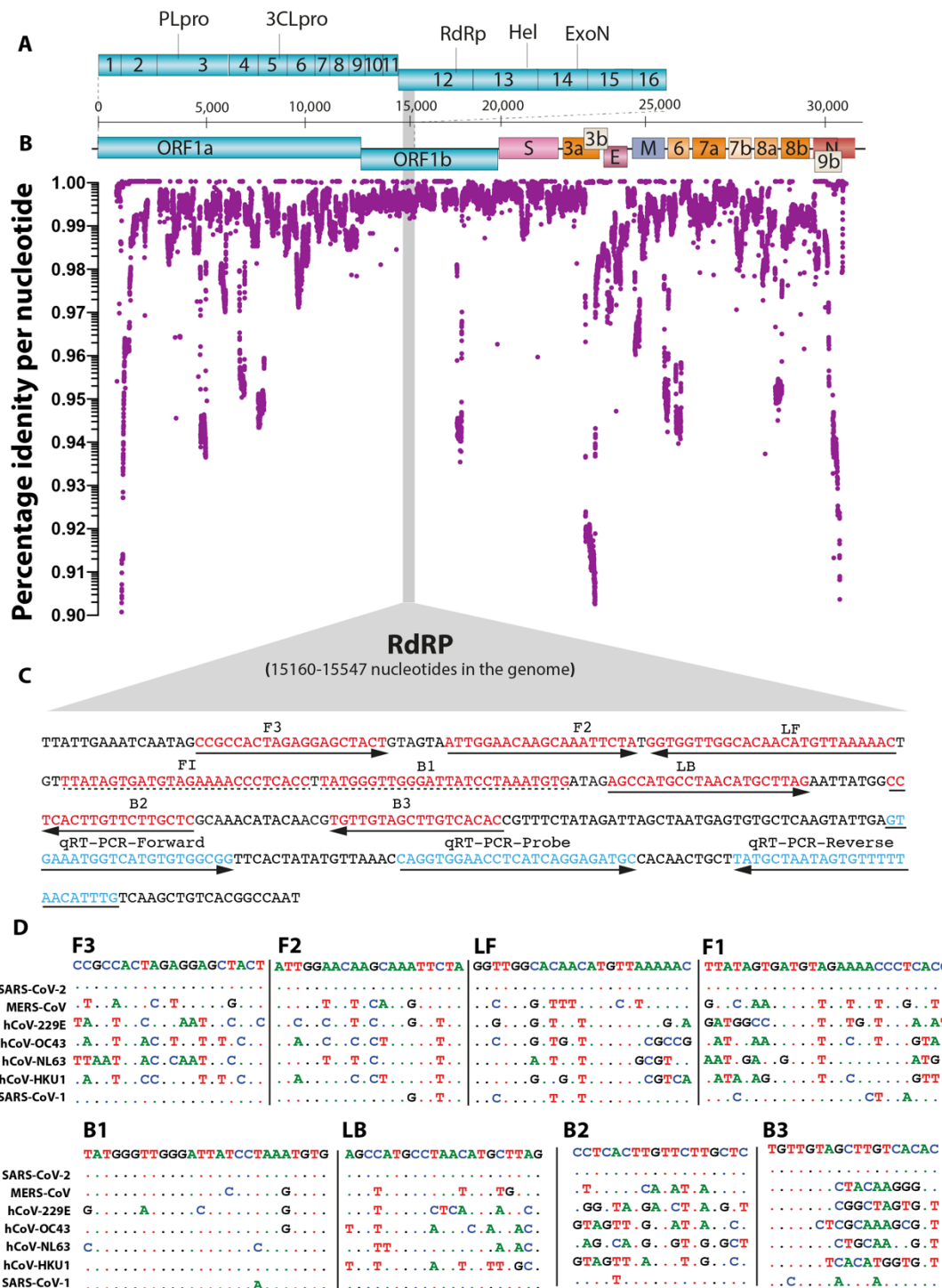
634 [11] Vogels CBF, Brito AF, Wyllie AL, et al. Analytical sensitivity and efficiency  
635 comparisons of SARS-COV-2 qRT-PCR assays. medRxiv.  
636 2020;2020.03.30.20048108. Available  
637 from: <https://medrxiv.org/content/early/2020/04/01/2020.03.30.20048108>.

638 [12] Kashir J and Yaqinuddin A. Loop mediated isothermal amplification (LAMP)  
639 assays as a rapid diagnostic for COVID-19. *Medical Hypotheses*. 2020;141.  
640 doi:10.1016/j.mehy.2020.109786.

- 641 [13] Yan C, Cui J, Huang L, et al. Rapid and visual detection of 2019 novel coronavirus  
642 (SARS-CoV-2) by a reverse transcription loop-mediated isothermal amplification  
643 assay. *Clin Microbiol Infec.* 2020 June; 26(6):773-779.
- 644 [14] Mori Y and Notomi T. Loop-mediated isothermal amplification (LAMP): Expansion  
645 of its practical application as a tool to achieve universal health coverage. *J Infect*  
646 *Chemother.* 2020 Jan;26(1):13-17.
- 647 [15] Mahony J, Chong S, Bulir D, et al. Development of a sensitive loop-mediated  
648 isothermal amplification assay that provides specimen-to-result diagnosis of  
649 respiratory syncytial virus infection in 30 minutes. *J Clin Microbiol.* 2013  
650 Aug;51(8):2696-701.
- 651 [16] Ganguli A, Ornob A, Yu H, et al. Hands-free smartphone-based diagnostics for  
652 simultaneous detection of Zika, Chikungunya, and Dengue at point-of-care. *Biomed*  
653 *Microdevices.* 2017 Aug 22;19(4):73.
- 654 [17] Kaarj K, Akarapipad P, Yoon JY. Simpler, Faster, and Sensitive Zika Virus Assay  
655 Using Smartphone Detection of Loop-mediated Isothermal Amplification on Paper  
656 Microfluidic Chips. *Sci Rep.* 2018 Aug 18;8(1):1-11.
- 657 [18] Yu L, Wu S, Hao X, et al. Rapid colorimetric detection of COVID-19 coronavirus  
658 using a reverse transcriptional loop-mediated isothermal amplification (RT-LAMP)  
659 diagnostic platform: iLACO. *Clin Chem.* 2020; 0:0,1–3, doi:10.1093/clinchem/hvaa102
- 660 [19] Nguyen T, Bang DD, Wolff A. 2019 Novel coronavirus disease (COVID-19):  
661 Paving the road for rapid detection and point-of-care diagnostics. *Micromachines*  
662 (Basel). 2020 March;11(3):306.
- 663 [20] Katoh K, Rozewicki J, Yamada KD. MAFFT Online Service: Multiple Sequence  
664 Alignment, Interactive Sequence Choice and Visualization. *Brief Bioinform.* 2019 Jul  
665 19;20(4):1160-1166.
- 666 [21] Sun Y, Mao X, Hong S, et al. Template Matching-Based Method for Intelligent  
667 Invoice Information Identification. *IEEE Access.* 27 February 2019;7:28392-28401.
- 668 [22] Yang G, Li H, Zhang L, et al. Research on a skin color detection algorithm based  
669 on selfadaptive skin color model; 2010 International Conference on Communications  
670 and Intelligence Information Security, Nanning, China. *IEEE Xplore.* 2010; 266-270.
- 671 [23] Al-Tairi, ZH, Rahmat RWO, Saripan MI, et al. Skin Segmentation Using YUV and  
672 RGB Color Spaces. *J Inf Process Syst.* 2014 June;(10)2: 283-299.
- 673 [24] Sharif M, Khan MA, Rashid M, et al. Deep CNN and geometric features-based  
674 gastrointestinal tract diseases detection and classification from wireless capsule  
675 endoscopy images. *J Ex Theor Artif In.* 01 Feb 2019 Feb,  
676 [doi.org/10.1080/0952813X.2019.1572657](https://doi.org/10.1080/0952813X.2019.1572657)
- 677 [25] WHO, Coronavirus disease (COVID-19) pandemic 2020b.  
678 <https://www.who.int/emergencies/diseases/novel-coronavirus-2019>
- 679 [26] Kurosaki Y, Grolla A, Fukuma A, et al. Development and evaluation of a simple  
680 assay for Marburg virus detection using a reverse transcription-loop-mediated  
681 isothermal amplification method. *J. Clin. Microbiol.* 2010 April 26; 48:2330–2336.
- 682 [27] Ge Y, Wu B, Qi X, et al. Rapid and sensitive detection of novel avian-origin  
683 influenza A (H7N9) virus by reverse transcription loop-mediated isothermal  
684 amplification combined with a lateral-flow device. *PLoS One.* 2013 Aug  
685 1;8(8):e69941.
- 686 [28] Kwallah A, Inoue S, Muigai AW, et al. A real-time reverse transcription loop-  
687 mediated isothermal amplification assay for the rapid detection of yellow fever virus.  
688 *J. Virol. Methods.* 2013 Oct;193(1):23-7.

689 [29] Cao Z, Wang H, Wang L, et al. Visual detection of west nile virus using reverse  
690 transcription loop-mediated isothermal amplification combined with a vertical flow  
691 visualization strip. *Front. Microbiol.* 2016 Apr 20;7:554.  
692 [30] Xu C, Wang H, Jin H, et al. Visual detection of Ebola virus using reverse  
693 transcription loop-mediated isothermal amplification combined with nucleic acid strip  
694 detection. *Arch. Virol.* 2016 May;161(5):1125-33.  
695 [31] Chotiwan N, Brewster CD, Magalhaes T, et al. Rapid and specific detection of  
696 Asian- and African- lineage Zika viruses. *Sci. Transl. Med.* 2017 May  
697 3;9(388):eaag0538.  
698 [32] Chen L, Liu W, Zhang Q, et al. RNA based mNGS approach identifies a novel  
699 human coronavirus from two individual pneumonia cases in 2019 Wuhan outbreak.  
700 *Emerg Microbes Infect.* 2020; 9(1): 313–319.  
701 [33] Lu R, Zhao X, Li J, et al. Genomic characterisation and epidemiology of 2019  
702 novel coronavirus: implications for virus origins and receptor binding. *The Lancet.*  
703 2020 February 22;395:565–574.  
704 [34] Chan JF, Yip CC, To KK, et al. Improved molecular diagnosis of COVID-19 by the  
705 novel, highly sensitive and specific COVID-19-RdRp/Hel real-time reverse  
706 transcription-PCR assay validated in vitro and with clinical specimens. *J Clin*  
707 *Microbiol.* 2020 Apr 23;58(5):e00310-20.  
708 [35] Wei M, Yuan J, Liu Y, et al. Novel coronavirus infection in hospitalized infants  
709 under 1 year of age in China. *JAMA.* 2020;323(13):1313-1314.  
710 [36] Shahid, M, Amin, I, Afzal, S, Fatima Z, Idrees, M. Comparative Analysis of  
711 Immunological and Genomic Outcomes of Dengue Virus Outbreak in Pakistan.  
712 *Pakistan J. Zool.*, Vol. 51, Iss. 5, pp 1971-1974  
713 [37] Sodi, R, Eastwood, J, Caslake, M, et al. Relationship Between Circulating  
714 microRNA-30c With Total- And LDL-cholesterol, Their Circulatory Transportation and  
715 Effect of Statins. *Clin Chim Acta.* 2017 Mar;466:13-19  
716  
717  
718  
719  
720  
721  
722  
723  
724  
725  
726  
727  
728  
729  
730  
731  
732  
733  
734  
735  
736  
737  
738

739



740

741

742

743

744

745

746

747

748

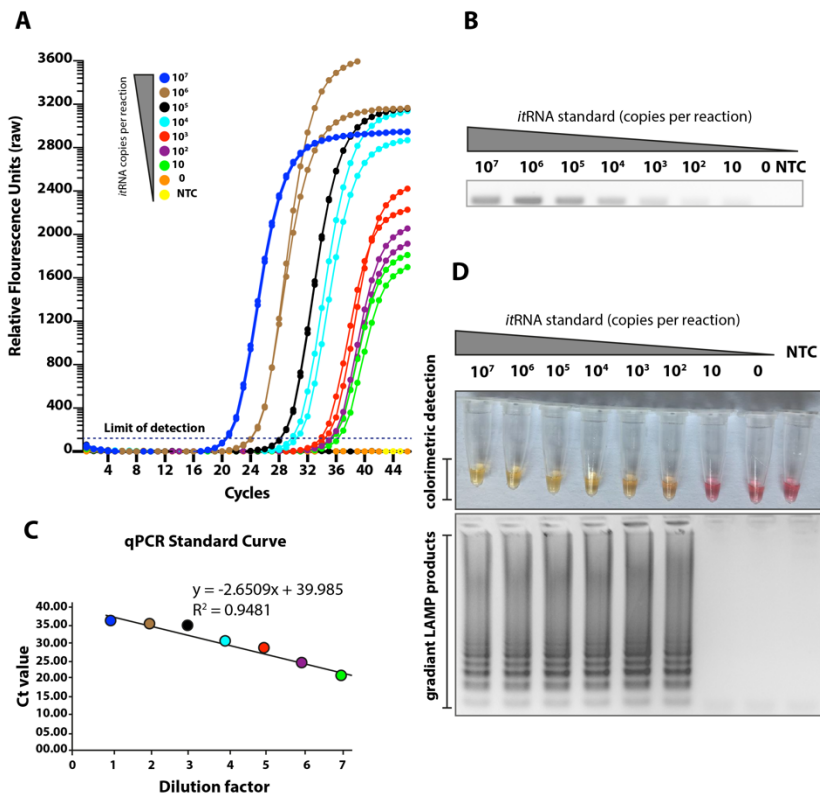
749

750

**Figure 1: In silico analysis of SARS-CoV-2 and primer design. (A)** Genome organization of SARS-CoV-2. Scale represents an approximate position of the genome whereas ORF1a and b are expanded to show internal gene organization. **(B)** Level of gene identity across the genome of the SARS-CoV-2. Identity less than 90% is not shown. **(C)** Primer location in the RdRp gene of SARS-CoV-2 is shown. Red coloured sequences represent LAMP primers whereas blue coloured sequences are primers and probes used in the qRT-PCR. **(D)** Comparative sequence identity using the primers against different human coronaviruses compared to the reference SARS-CoV-2 sequence; dots represent identical nucleotides.



751



752

753

754 **Figure 2: Sensitivities of the LAMP assay.** (A) Seven different dilutions of in vitro  
 755 transcribed RNA were run for quantitatively measurement in the qRT-PCR. Relative  
 756 fluorescence units show a gradient decrease in signals. (B) The corresponding PCR  
 757 products on the electrophoresis gel (C) The qRT-PCR standard curve based on the  
 758 Ct value and dilution factor. (D) The serially diluted synthetic RNAs were run for LAMP  
 759 assay and colour change represents positive (yellow) or negative (pink). The lower  
 760 panel show LAMP gradient products.

761

762

763

764

765

766

767

768

769

770

771

772

773

774

775

776

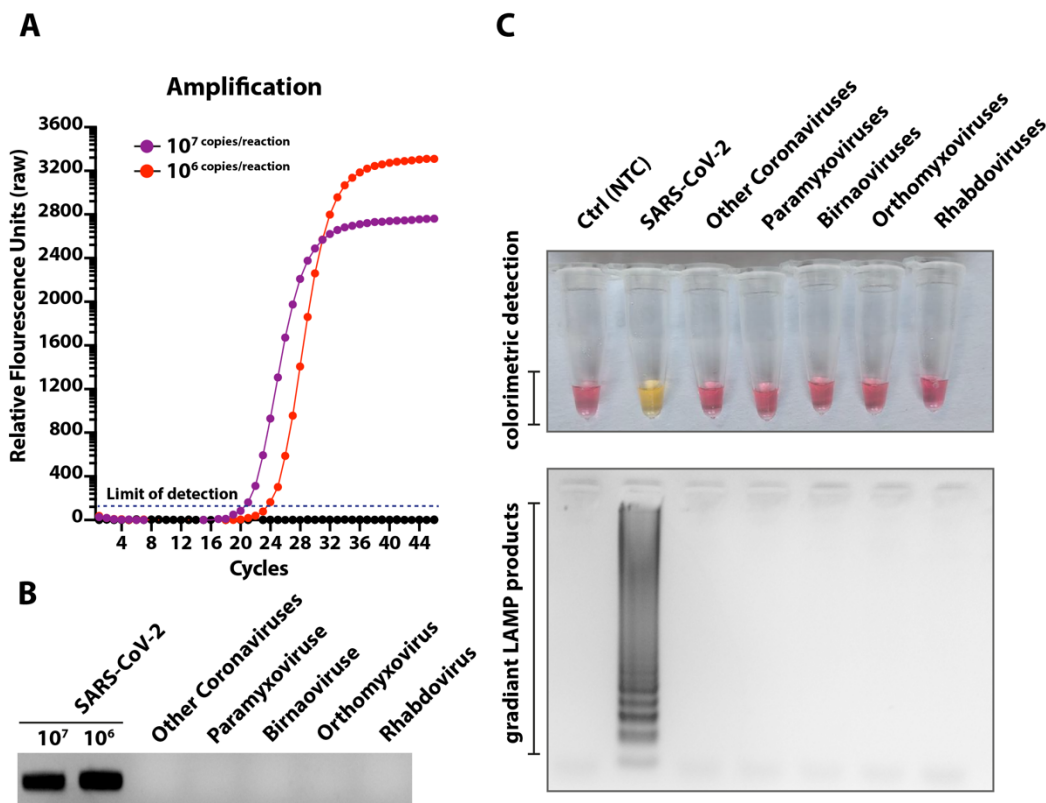
777

778

779

780

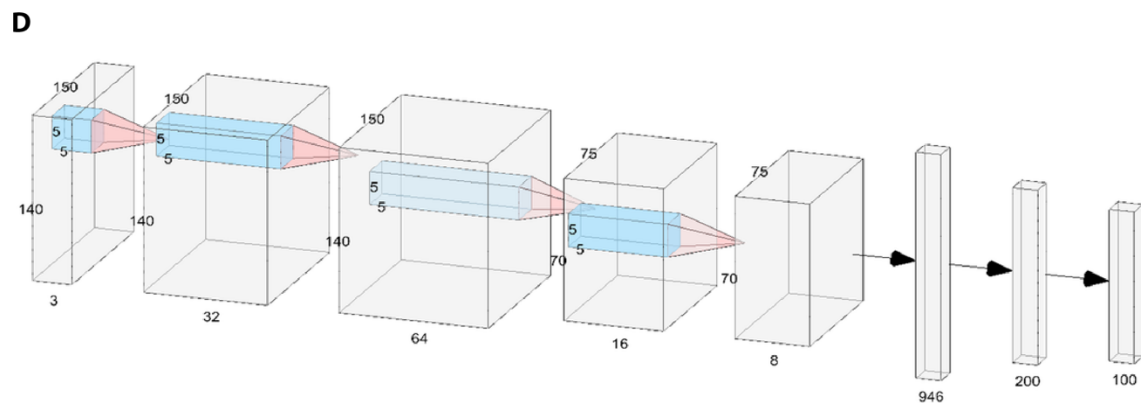
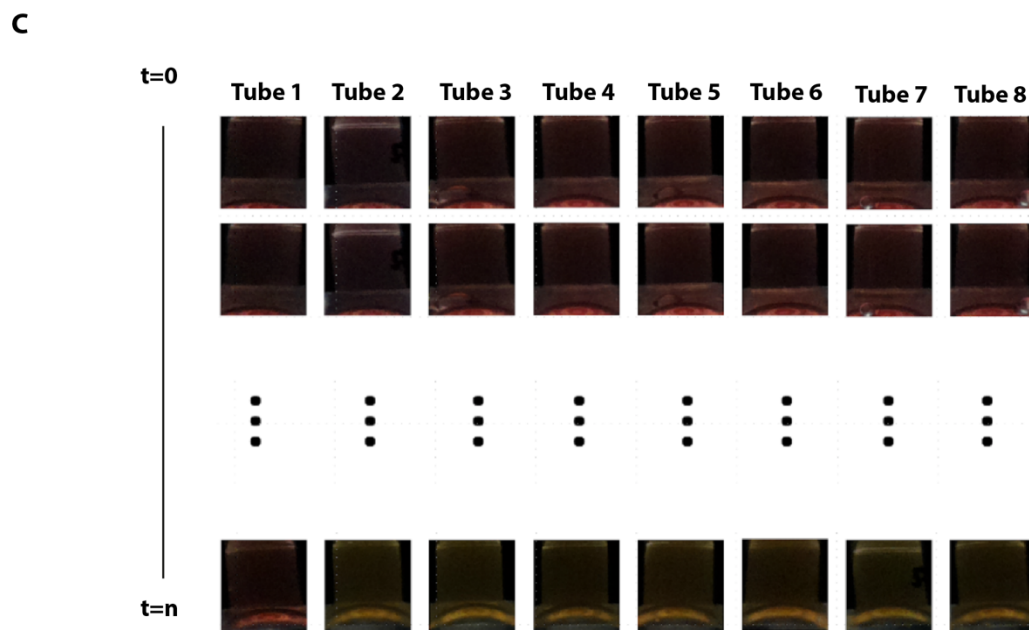
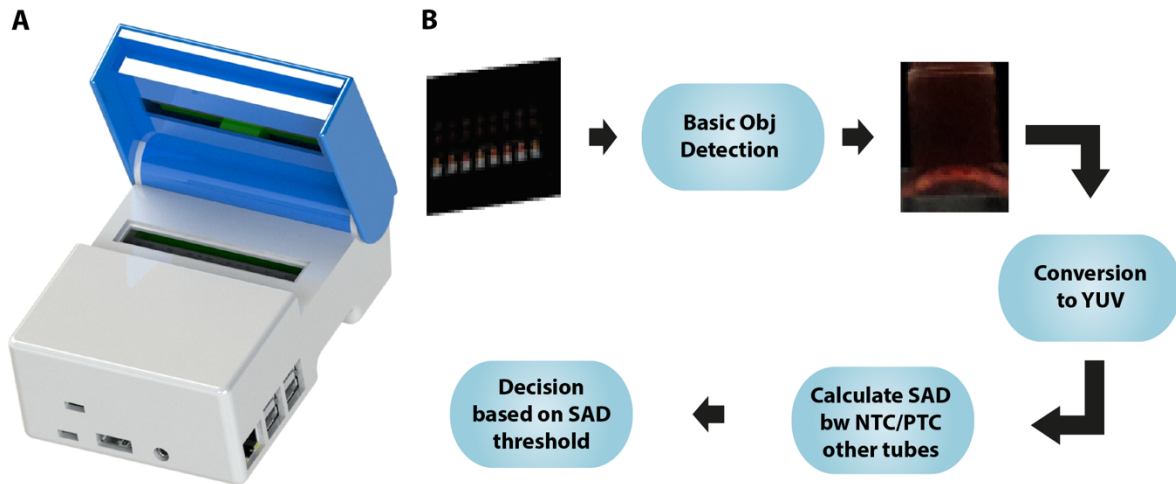
781  
782



783  
784  
785  
786  
787  
788  
789  
790  
791  
792  
793  
794  
795  
796  
797  
798  
799  
800  
801  
802  
803  
804  
805  
806  
807  
808  
809

**Figure 3: Specificity of the LAMP assay.** (A) RNA extracted from different medically or respiratory important viruses as well as two dilutions of synthetic RNA were run for qPCR. (B) Corresponding PCR products were run on gel to demonstrate specificity. (C) Similar to qRT-PCR, extracted RNA were run for the LAMP assay. The top panel indicates the colorimetric detection of LAMP positive/negative reactions and the lower panel show the electrophoresis of the corresponding LAMP products.

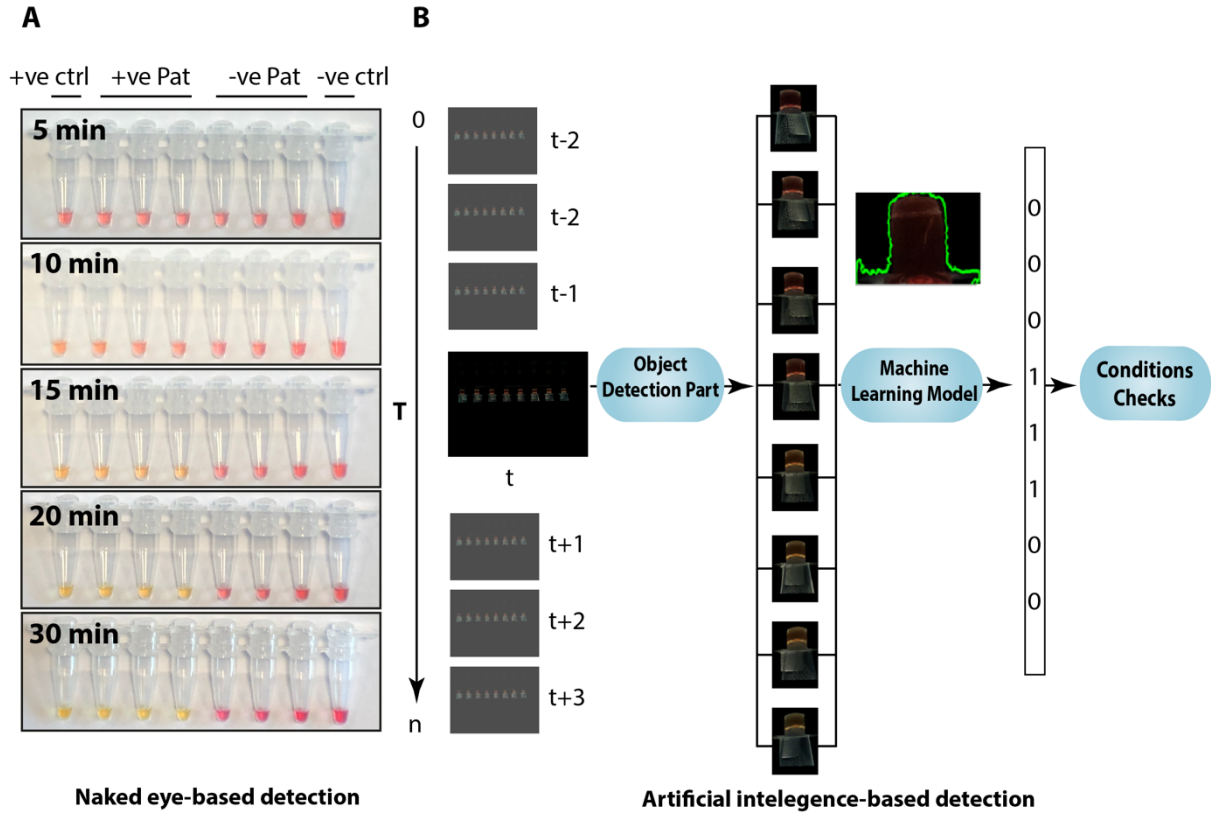
810



811  
812  
813  
814  
815  
816  
817

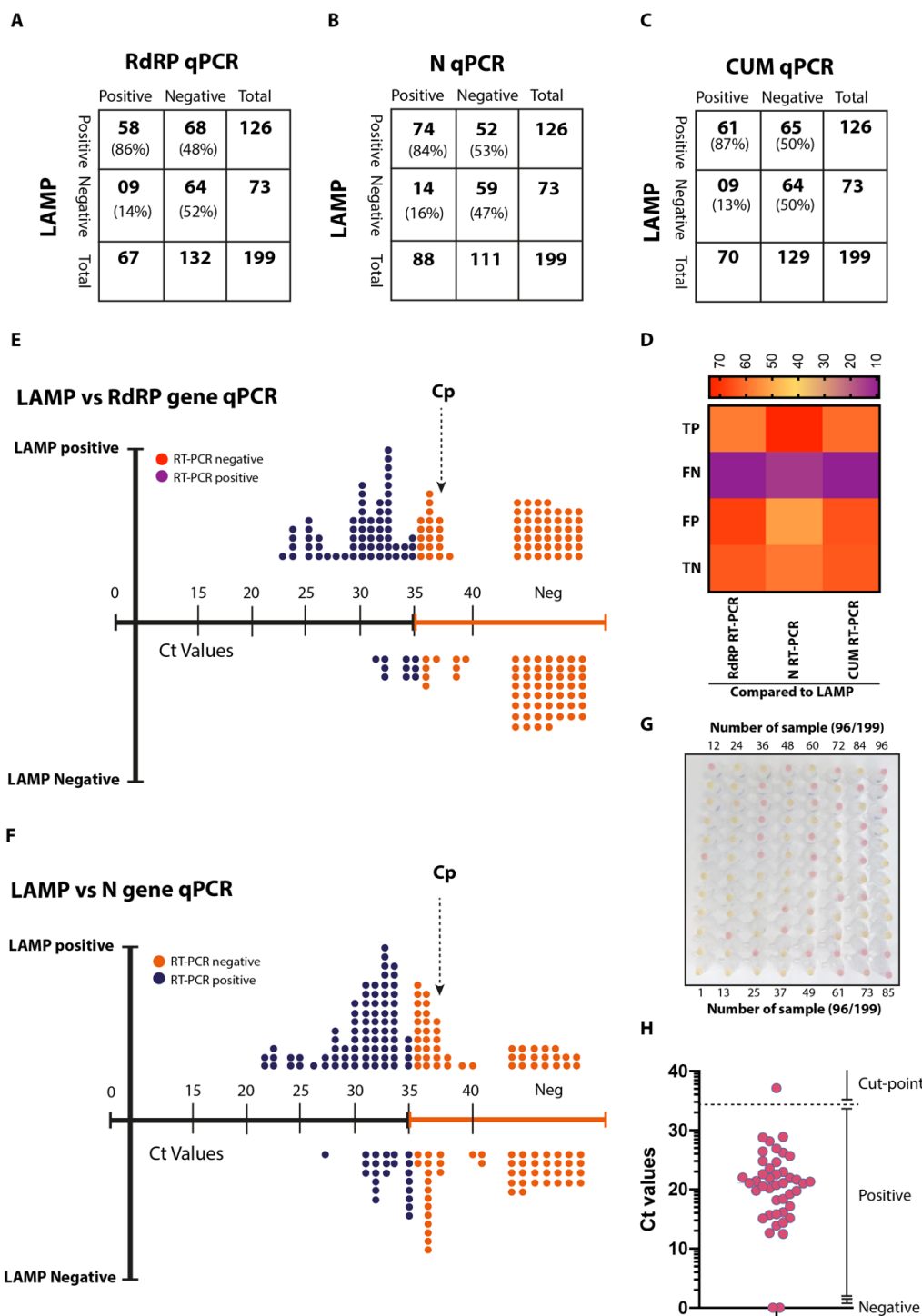
**Figure 4: Fabrication and processing of LAMP data for enhanced detection of SARS-CoV-2. (A)** Exterior of a smart diagnostic device **(B)** Description of the AI-assisted algorithm and image processing. **(C)** Pipeline to process images and extraction of colorimetric information. **(D)** Schematic outlining the training of the network for image processing.

818



819  
820  
821  
822  
823  
824  
825

**Figure 5: Conventional and AI-assisted interpretation of LAMP results. (A)** Temporal analysis of known positive and negative patient samples for visual interpretation of LAMP results. **(B)** Interpretation of corresponding patient samples by the AI-assisted LAMP results.



826  
827  
828  
829  
830  
831  
832  
833  
834  
835  
836  
837

**Figure 6: Clinical validation of ai-LAMP.** (A-C) Comparative sample positivity between LAMP and RdRP qRT-PCR (A), LAMP and N qRT-PCR (B), LAMP and CUM qRT-PCR results (C). (D) The heatmap indicate the relative positive and negative samples among three assays. (E) Linearity chart comparing the LAMP positive/negative samples and their detection based on the RdRP gene-based qRT-PCR. (F) Linearity chart comparing the LAMP positive/negative samples and their detection based on the N gene-based qRT-PCR. (G) Naked eye detection of first 96 samples out of the total 199 patients' samples processed. (H) Recovery Ct values of the miRNA from spiked before RNA extraction.